16th International Conference on Greenhouse Gas Control Technologies, GHGT-16

23rd-27th October 2022, Lyon, France

Performance analysis of pressure swing adsorption process for carbon-containing off-gas separation in the steel industry

Fidal Bashir, Richard T. J. Porter, Elena Catalonotti, Haroun Mahgerefteh*

Department of Chemical Engineering, University College London, London WC1E 7JE, United Kingdom

Abstract

This work aims to model the implementation of Pressure Swing Adsorption (PSA) to recover CO_2 from Blast Furnace Gas (BFG), CO from Basic Oxygen Furnace Gas (BOFG) and H_2 from Coke Oven Gas (COG). Three independent PSA units are modelled using Aspen Adsorption, with each system fitted with different adsorbents, specific designs and configurations for the desired outlet gas. A layered bed PSA packed with activated carbon and Zeolite 5A adsorbent recovers H_2 from COG, achieving 99.3 vol% purity and >90% recovery. A Vacuum Pressure Swing Adsorption (VPSA) was employed to analyse CO recovery from BOFG using a copper chloride-impregnated Activated Carbon (CuCl/AC) adsorbent to achieve a 98 vol% purity and >90% recovery. Finally, the simulation and optimisation studies for CO_2 recovery from BFG, using commercial Zeolite 13X as the adsorbent to achieve a 96% purity stream with >90% recovery. Model validation was performed by comparing the simulation results for breakthrough with relevant experimental data. Furthermore, a parametric study was carried out to determine the purity of PSA systems for gas separation from different steelworks off-gases.

Keywords: Adsoprtion; PSA; VPSA; process simulation.

Nomenclature

A_W = cross-sectional area of the wall, cm^2
Cpg = gas heat capacity, cal/g K
Cpw = wall heat capacity, cal/g K
D_L = axial dispersion coefficient, cm^2/s
D_{mi} = molecular diffusivity, cm^2/s
dp = particle diameter, cm
$-\Delta H$ = average heat of adsorption, cal/mole
hi,o= internal and outer heat transfer coefficient, cal cm^{-2} K^{-1} s^{-1}
IP = isotherm parameter, kmol kg^1 bar^{-1})
K_L = axial thermal conductivity, cal cm^{-1} s^{-1} K^{-1}

* Corresponding author. *Email address:* h.mahgerefteh@ucl.ac.uk

P = total pressure, bar
P_i = partial pressure, bar
q_i = average amount adsorbed, mol/g
R = gas constant, cal mol^{-1} K^{-1}
Re = Reynolds number (-)
R_{Bi} = bed inside radius, cm
R_{Bo} = bed outside radius, cm
Sc = Schmidt number (-)
t= time, s
T_{atm} = atmospheric temperature, K
T = pellet or bed temperature, K
T_w = wall temperature, K
u = interstitial velocity, cm/s
v = fluid dynamic viscosity, Pa s
y_i = mole fraction of species i
z = axial distance in bed from the inlet, cm

Greek symbols
ε = voidage of adsorbent bed (-)
ρ_g = gas density, g/cm^3
ρ_p = pellet density, g/cm^3
ρ_W = bed wall density, g/cm^3

1. Introduction

Energy intensive industry was responsible for almost a quarter of CO_2 emissions in 2017 [1]. The cement and steel subsectors are the highest CO_2 emitters. Coal is a primary energy resource for iron production and its derivative, coke, is used as a reducing agent in blast furnaces. The direct emissions from fossil fuel usage related to steel production (2.1 $GtCO_2$) is about 7-9% globally [1]. Therefore, the emissions from steel production should be reduced by 1.5–0.75 Gt CO_2/yr to keep on track based on the Paris agreement timeline for achieving net zero emissions by 2050 [2].

1.1 Steel Production and CCUS

The Blast Furnace – Basic Oxygen Furnace (BF-BOF) route dominates steel production and its energy consumption contributes to about 70% used in this sector. The process is responsible for about 74.3% of all steel production globally [3]. The efforts to reduce carbon emissions by the European Steel Association are focused on CCUS without altering the original route to steel production [4]. However, future forecasts suggest that BF-BOF route will remain the main steel production route, with an estimate of more than 50% of the total steel produced in 2050. Therefore, focusing on the integrated steel mill route is significant as the off-gases storage and utilisation will be very important [4].

The three main steelworks off-gases produced as a result of the steel-making process are Blast Furnace Gas (BFG), Coke Oven Gas (COG) and Basic Oxygen Furnace Gas (BOFG). The largest flow in an integrated steelworks by far is for BFG, which comprises ~85% of the total gases produced. Given the pressing need to reduce carbon emissions from the steel industry, the carbon-containing off-gases produced during the steel manufacturing process can potentially be valorised via conversion into valuable products such as commodity chemicals without altering the steel production route. Such efforts to utilise these steel off-gases generated continuously and inherently have attracted global attention [5]. The major components of these off-gases are N_2, CO_2, CO, CH_4 and H_2, which constitute the three main off-gases in different proportions.

Table 1 shows each gas stream's composition, typical flow rate, thermal power, and Lower Heating Value (LHV) for a modern steel plant. BFG is rich in N_2 since air is used as an oxidant in blast furnaces. Unlike COG, BFG has a considerably smaller amount of H_2. Coke's oxidation generates other compounds such as CO and CO_2 in this stream to reduce the iron ore and enhance the furnace temperature. The basic oxygen furnace, where iron in molten form

reacts with pure O_2 to remove impurities (residual carbon and other metals) is where the BOFG is generated. BOFG is rich in CO and is often used as feed gas to the BF, as an additional reducing agent to coke. Given the energy content stored in some of these gases, they are traditionally utilised within the plant as fuels to generate electricity and meet the overall process energy demands.

Table 1. Typical stream compositions, flow rate, and Lower Heating Values of exhaust gases after cleaning in a steel plant [6,7].

Compound	**BOFG**	**BFG**	**COG**
CO	58	20	6
CO_2	20	24	2
H_2	4	3	63
N_2	18	53	4
CH_4	0	0	25
Density	1.38	1.40	0.42
Volumetric flow rate (Nm^3/h)	35,000	730,000	40,000
Thermal power (MW)	70	682	174
LHV (MJ/Nm^3)	7.6	2.85	17.5

The gases are also typically used as fuel to heat the rolling mill or provide heat and power in a combined heat and power plant [6]. However, in addition, these gases may be processed to create useful chemicals (e.g. methanol) [8] and for CO_2 capture and storage application. Therefore, for the gases to be utilised, they must be separated and conditioned for specific applications. A suitable technology to separate the individual components of these gases for either utilisation or storage is Pressure Swing Adsorption (PSA). Adsorption-based technologies have the potential to be used in all CO_2 capture categories, including post-combustion capture, pre-combustion capture, oxy-combustion, natural gas sweetening, and negative emissions (i.e., direct-air capture) [9].

1.2 Pressure Swing Adsorption (PSA)

PSA is designed based on the basic principle of adsorption and generally works through separation of heavier components (adsorbates) from lighter components (raffinates) in a feed stream. The PSA process is typically applied in gas-solid systems at the absorbent surface to achieve rapid adsorption as well as desorption via bed pressure alteration from high to low. The adsorbent is selected based on its affinity to the desired adsorbate in the feed stream. During the adsorption, the pressure is adjusted to the maximum to enhance the take-up of adsorbate, resulting in a product stream rich in the lighter components in the gas phase. Following the adsorbent's near saturation with adsorbate, the bed pressure is reduced, allowing the adsorbed species to desorb back to the gas phase in a process known as regeneration.

Adsorption isotherms are used to help predict the behaviour of the adsorption process. These curves show a component's retention potential in the solid phase while it is at equilibrium, with various isotherm models being applied [10]. Comparing process and design variables is a major exercise in PSA performance assessment. Purity, recovery and productivity are used to determine separation mixtures' efficiency when using PSA [11].

1.2.1 Breakthrough curves

The adsorption step in the PSA cycle is crucial, especially when the system needs to be optimised. It is fundamental for optimal PSA design to analyse adsorption dynamics and breakthrough behaviour based on the feed mixture. The breakthrough curve provides information on the amount of substance adsorbed during the PSA process and the saturation point of the adsorbent.

1.2.2 Adsorbents

In the design of a PSA system, certain factors such as the screening of adsorbent materials are of paramount importance as the PSA's performance hinges on their selection. PSA typically uses Activated Carbons (ACs), silica gels, zeolites, and activated aluminas as adsorbents [12]. In comparison to other adsorbents, ACs have a higher CO_2 adsorption capacity. Also, they are very competitive because of their cost-effective price, large surface area that can be altered via the capability to change pore structure [13]. Zeolites posses an open crystal lattice, with uniform micropore structure and without any pore size distribution. Zeolites are distinguished from other adsorbents by this feature [14] and have exceptional adsorption properties. Due to their honeycomb structure, they have the ability to bind some contaminants permanently. They are also easily accessible and can be utilised in various adsorbent systems. Various works have been conducted for the separation of H_2 from syngas using a layered bed of AC, zeolites and alumina [15–17] to achieve high purity level for H_2 to be utilised as fuel. Works from Gao *et al.* [18] and Abdeljaoued *et al.* [19] prepared an AC supported CuCl adsorbent for CO separation from syngas using VPSA modelled in Aspen Adsorption; the adsorbent showed good CO adsorption capacity and reversibility. There are also several works for high purity CO_2 production using zeolites especially 13x and 5A; these works have shown favourable results in terms of product recovery and purity [20].

2. Methodology

2.1 Model assumptions

Material, energy, and momentum balances are used in the mathematical model for dynamic simulation of an adsorption bed. A schematic of the PSA systems is shown in Fig. 1. A PSA system fundamentally consists of two or more adsorbent beds; these beds are connected to each other through valves, which control the system's operation. To ensure a continuous gas stream flow, a multiple bed system is used. The PSA configuration applied for all PSAs in this work is the Skartstrom cycle. The Skartsrom cycle or a variation of it is the most commonly applied PSA configuration. The cycle involves two beds performing concurrent feed pressurisation, feed adsorption, counter-current based blowdown, and counter-current based purge with the product [21]. Fig. 1 below shows the mode of operation of a typical Skartsrom cycle PSA system.

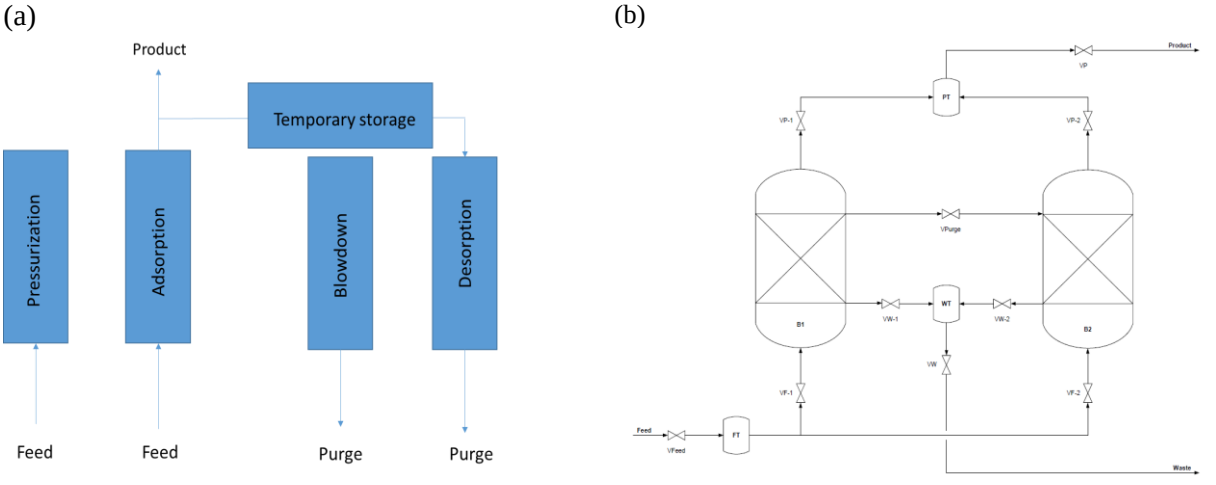

Fig. 1. PSA bed configuration, (a) 2-bed, 4-step Skartsrom cycle [22] and (b) generalised PFD of a PSA.

For the present case studies, a typical configuration of a Two-Bed, Four-Step (2B4S) Skarstrom cycle PSA set-up was adopted, which employs the following or similar type of sequenced steps:

1. Pressurise Bed 1; Blowdown Bed 2 (PR-B1; BD-B2)

2. Adsorption Bed 1; Purge Bed 2 (AD-B1; PG-B2)

2. Blowdown Bed 1; Pressurise Bed 2 (BD-B1; PR-B2)

3. Purge Bed 1; Adsorption Bed 2 (PG-B1; AD-B2)

The sequenced steps for the basic cycle involves the high pressure feed gas stream being fed Bed 1, where first pressurisation of Bed 1 takes place, and once the bed is adequately pressurised, the gas components that are not preferentially adsorbed on the bed, pass through and are collected as the product gas stream. After the bed is nearly saturated with the preferred component, the next set of steps bring about the de-pressurisation of the bed during the blowdown process. Once the bed has been essentially regenerated, it is expected to be re-pressurised with the residual pressure for the feed gas. Fig. 1 shows a simplified process flow diagram (PFD) of a generalised PSA. The Skartstrom cycle variation applied in this work is presented in Table 2.

Table 2: Variation of Skartsrom cycle PSA steps applied.

		Time, s		
Step #	**Step**	**PSA-I (H_2)**	**PSA-II (CO)**	**PSA-III (CO_2)**
1	AD-B1; PG-B2	100	30	185
2	BD-B1; PR-B2	20	120	15
3	PG-B1; AD-B2	100	30	185
4	PR-B1; BD-B2	20	120	15

In this study, the Linear Driving Force (LDF) model with a single lumped mass transfer parameter describes the sorption rate into an adsorbent pellet in the bed. One of the most widely used isotherm models is the Langmuir adsorption model, which describes gas-solid phase adsorption and is also used to quantify and contrast the adsorptive capacity of various adsorbents. The Langmuir isotherm accounts for surface coverage by balancing the relative adsorption and desorption rates (dynamic equilibrium) [23]. The model describes adsorption by assuming an adsorbate behaves as an ideal gas at isothermal conditions.

Table 3: PSA model equations

Equation	**Performance measured**	**Definition**
1	Mass balance	$-\mathrm{D_L}\frac{\partial^2 \mathrm{y_i}}{\partial \mathrm{z}^2}+\mathrm{u}\frac{\partial \mathrm{y_i}}{\partial \mathrm{z}}+\frac{\partial \mathrm{y_i}}{\partial \mathrm{z}}+\rho_\mathrm{P}\frac{\mathrm{RT}}{\mathrm{P}}\left(\frac{1-\varepsilon}{\varepsilon}\right)\left(\frac{\partial \mathrm{q_i}}{\partial \mathrm{t}}-\mathrm{y_i}\sum_{\mathrm{i=1}}^{\mathrm{n}}\frac{\partial \mathrm{q_i}}{\partial \mathrm{t}}\right)=0$
2	Wall energy balance	$-\rho_\mathrm{W}\mathrm{C_{PW}}\mathrm{A_W}\frac{\partial \mathrm{T_W}}{\partial \mathrm{t}}=2\pi\mathrm{R_{Bi}}\mathrm{h_i}(\mathrm{T}-\mathrm{T_W})-2\pi\mathrm{R_{BO}}\mathrm{h_O}(\mathrm{T_W}-\mathrm{T_{atm}})$
3	Energy balance	$K_L\frac{\partial^2 T}{\partial z^2}+\varepsilon\rho_g C_{pg}\left(u\frac{\partial T}{\partial z}+T\frac{\partial u}{\partial z}\right)+\left(\varepsilon_t\rho_g C_{pg}+\rho_B C_{pg}\right)\frac{\partial T}{\partial t}-\rho_{\boldsymbol{Bu}}(-\Delta H_i)\sum_{i=1}^{n}\frac{\partial q_i}{\partial t}+\frac{2h_i}{R_{Bi}}(T-T_W)=0$
4	Pressure drop across the bed	$\frac{\partial \mathrm{P}}{\partial \mathrm{z}}-150\mathrm{v}\,\frac{(1-\varepsilon_\mathrm{b})^2\mathrm{u}}{\varepsilon_\mathrm{b}{}^3\mathrm{d_p}{}^2}-\frac{1.75(1-\varepsilon_\mathrm{b})\rho\mathrm{u}\lvert\mathrm{u}\rvert}{\varepsilon_\mathrm{b}{}^3\mathrm{d_p}}=0$
5	Axial dispersion coefficient	$\frac{\varepsilon_b D_L}{\mathrm{D_m i}}=20+0.5\,\mathrm{Sc}\,\mathrm{Re}$

Using an axially dispersed plug flow reactor and applying the ideal-gas law, the material balance for the bulk phase in the adsorption column is given by equation 1. This work applies the following assumptions to a full dynamic model of PSA systems:

i. The axial dispersion plug flow model can be used to describe the flow pattern in the bed;
ii. the solid and gas phases reach thermal equilibrium instantly;
iii. radial concentration and temperature gradients in the adsorption bed are negligible; and
iv. axial conduction in the wall can be ignored.

To consider heat loss through a wall and heat accumulation in the wall, an energy balance for the wall of the adsorption bed was used (equation 2). This is needed because the extent of the temperature variation caused by the heat of adsorption greatly affects the overall adsorption process. This is why the energy balance for the gas-phase includes the heat transfer to the column wall. By assuming a thermal equilibrium between fluid and particles, the energy balance for gas and solid phases is given by equation 3. Ergun's equation (equation 4) was applied to determine the pressure drop across the bed. The axial dispersion coefficient (equation 5) is calculated through a correlation proposed by Wakao and Funazkri [24] which calculates the axial dispersion coefficients for every feed mixture component, making the diffusivities the only parameter required.

3. Simulation

Aspen Adsorption V10 is a modelling tool for identifying the best design and optimisation of cyclic adsorption processes for gas separation, such as PSA, Thermal Swing Adsorption (TSA) and VPSA, depending on the desired levels of purity and recovery. Aspen Adsorption was employed in the present study. The software uses a combination of partial differential equations, ordinary differential equations, and algebraic equations to extensively describe the adsorption process. These equations represent the mass, momentum, energy balances, kinetic and equilibrium models, and initial and boundary conditions. The bed and adsorbent conditions as input in Aspen Adsorption are presented in Table 4.

Table 4: Bed and adsorbent characteristics.

PSA system	**PSA-I** [25]		**PSA-II** [26]	**PSA-III** [27]
Adsorbent	AC	Zeolite 5A	AC-CuCl	Zeolite 13X
Bed length (m)	0.65	0.35	1	1.2
Bed diameter (m)	0.37		0.25	1.22
Bulk bed density (kg/m^3)	482	764	473	1256
Bed porosity	0.433	0.357	0.24	0.53
Adsorption pressure (bar)	8.5		1.2	1.5
Desorption pressure (bar)	1.0		0.07	0.4
Temperature (^{o}C)	25		25	25
Steps	4		4	4
Cycle time (s)	240		300	400

Adsorption isotherm data were fitted to Langmuir isotherm systems in Aspen, experimental isotherms from the literature were linearly regressed and adjusted to meet simulation and feed conditions.

3.1 H_2 separation from COG

For the separation of H_2 from COG feed, the adsorption bed configuration was based on the previous work by Ahn *et al*. [17], where a two-layered bed packed with AC and zeolite 5A was used to produce high-purity H_2 from syngas under high pressure. A product purity 99.3% and 90% recovery was obtained at 25°C, 8.5 bar adsorption pressure and 1 bar desorption pressure. The isotherm type used, along with the parameters utilised, are summarised in Table 5.

The PSA was simulated under pressure-driven mode, with the product's feed and bed pressures fixed. The feed temperature was kept at 25 °C. The type of isotherm used in the simulation was the Extended Langmuir – 3, as given by equation 6.

$$\omega_i = \frac{(IP_{1i} - IP_{2i}T_5)IP_{3i}e^{IP_{4i}/T_5}P_i}{1 + \sum_k(IP_{3k}e^{IP_{4k}/T_5}P_k)} \quad (6)$$

Table 5. Isotherm configuration for H_2 PSA.

Isotherm Type	**Extended Langmuir - 3**			
	Layer 1 (Activated Carbon)			
Component	**IP1**	**IP2**	**IP3**	**IP4**
CH_4	0.024	5.62E-05	0.003478	1159
CO	0.0335	9.07E-05	2.31E-05	1751
CO_2	0.02.E-02	7.00E-05	0.01	1030
H_2	01.69E-02	2.10E-05	6.25E-05	1229
N_2	1.6441	7.30E-04	0.0545	326
	Layer 2 (Zeolite 5A)			
CH_4	5.8E-03	1.19E-05	6.51E-04	1731
CO	1.2E-02845	3.13E-05	2.02E-02	763
CO_2	0.01	1.86E-05	1.58	207
H_2	0.4.3E-03	1.06E-05	2.52E-03	458
N_2	4.81	6.68E-03	5.70E-04	1531

Breakthrough curves were obtained for a layered bed of AC and Zeolite 5A and (0.65:0.35) at 10-atm adsorption pressure and 8.6 L/min feed rate. the simulated curves were validated against experimental results from Ahn *et al.* [17] with good agreement observed.

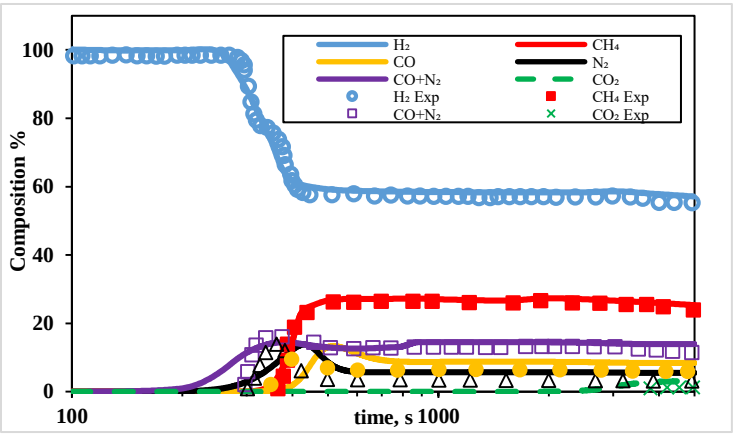

Fig. 2. Validation of a layered bed's breakthrough curves using Ahn *et al.*'s experimental data [25].

3.1.1. Parametric analysis

A pressure-based parametric analysis was carried out, where adsorption pressure was varied from 5.0 bar to 10.5 bar and its effect on H_2 purity in the product stream, was reported. Fig. 3 summarises the findings.

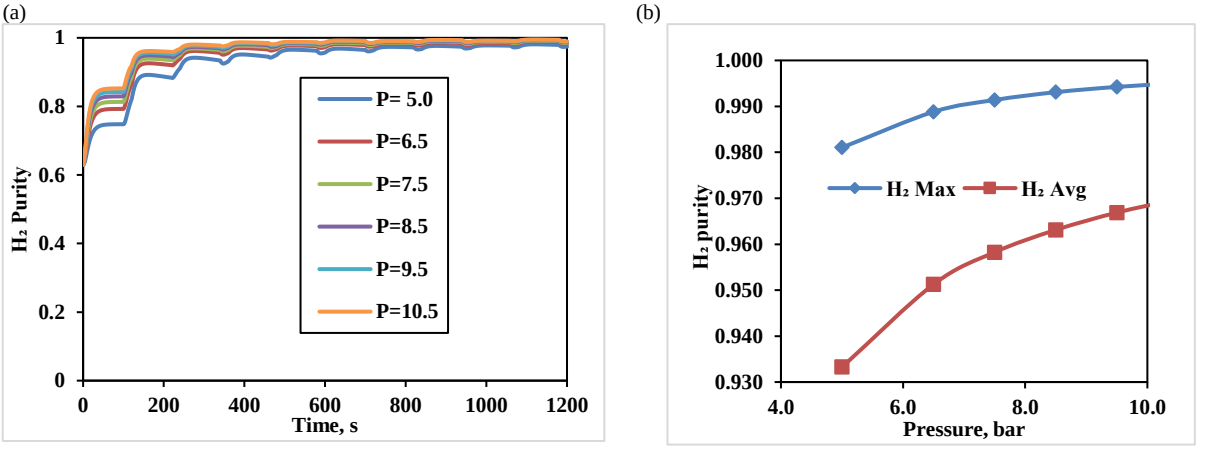

Fig. 3. (a) effect of adsorption pressure on H_2 purity and (b) effect of adsorption pressure on average and max H_2 purity.

It is observed that with high feed pressure, it is expected that all the other components except H_2 will be adsorbed by the two-layer bed system, resulting in high-purity H_2. Fig. 3 shows the effect of pressure on the maximum and average H_2 purity; it gives an overview of the effect of pressure on H_2 purity. From both figures 3(a) and 3(b) it could be concluded that although there is a slight improvement in H_2 purity when the pressure increases from 8.5 bar to 10.5 bar, the marginal increase in H_2 purity is only about 0.2 %. This necessitates the justification of marginal improvement in H_2 purity, with considerable pressure or compression costs. The effect of the feed temperature on H_2 purity was also analysed, the findings of which indicate that the H_2 purity essentially remains unaffected by the temperature increase and only shows marginal drop at a slightly higher temperature.

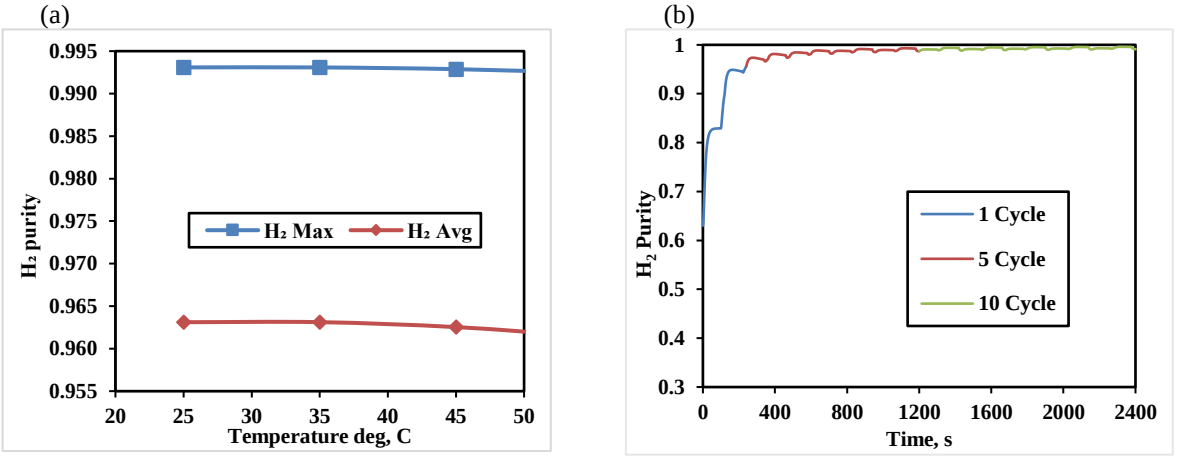

Fig. 4. (a) Effect of feed temperature on H_2 Purity and (b) effect of number of cycles on H_2 purity.

The number of cycles for the PSA was also varied, as shown in Fig. 4b. As expected, the 1-cycle PSA exhibited the poorest performance with respect to the H_2 purity (about 95.6 %), and the 10-cycle PSA gave the highest H_2 purity (99.3 %) (Fig. 4). This is because the simulation was run under dynamic state and the initial conditions where the bed is unsaturated with feed take some time to reach steady state. As in industrial applications, the unit runs continuously, it is safe to say the first few cycles will count for little in the overall product purity.

3.2 CO separation from BOFG

The CO adsorption bed configuration and isotherm parameters were based on the previous work by Gao *et al.* [26], where a single-layer bed was used to produce high-purity CO, albeit desorption under vacuum pressure conditions. These isotherms were adjusted and the bed was configured to meet feed gas specifications and conditions. For this work, breakthrough validation wasn't conducted due to lack of experimental data from open literature at the present conditions and mode of operation. The VPSA bed data was assimilated from the cited literature by Gao *et al.* [18]. A product purity of 99% and 91% recovery was obtained at adsorption pressure of 1.2 bar and desorption under vacuum pressure of 0.07 bar. The isotherm type used, along with the parameters utilised, are summarised in table 6 which follows:

Table 6: Isotherm configuration for CO VPSA.

Isotherm Type	**AC-Cu Langmuir - 1**	
Component	**IP1**	**IP2**
CH_4	1.79E-04	0.171
CO	0.013	3.551
CO_2	5.26E-04	0.228
H_2	4.52E-05	0.191
N_2	7.33E-05	0.215

The VPSA was simulated for the experimental isotherm parameters and flowrate conditions cited in literature [18], with the feed pressure, feed temperature, and bed pressure fixed. To investigate the vacuum conditions, the product stream or the waste stream pressures were varied to meet the product specifications. The type of isotherm used in the simulation was Langmuir – 1 as described in equation 7:

$$\omega_i = \frac{IP_1 P_i}{1 + IP_2 P_i} \qquad (7)$$

3.2.1 Parametric Analysis

The effect of the vacuum pressure on the CO purity was analysed, the vacuum pressure was varied from 0.07 bar to 0.2 bar and reveal the findings on the effect of the vacuum.

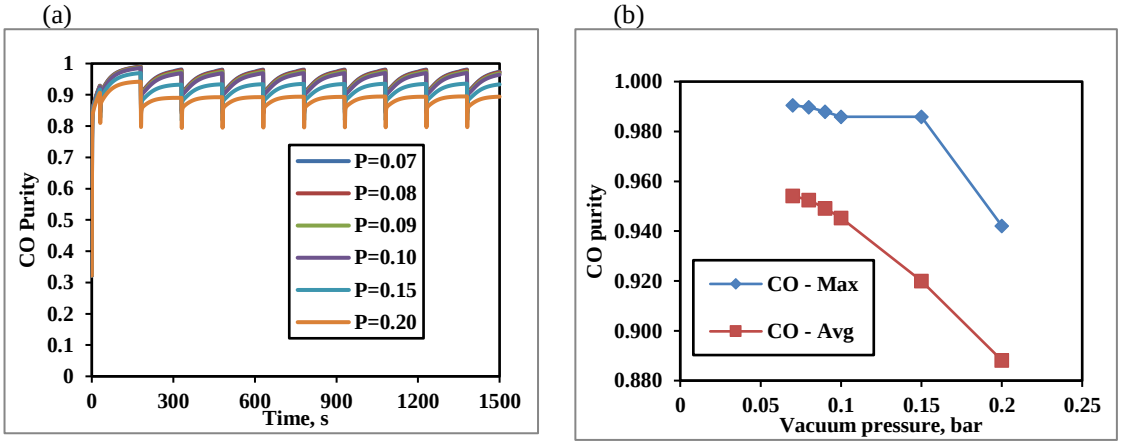

Fig. 5. (a) Effect of vacuum pressure on CO purity and (b) effect of vacuum pressure on maximum and average CO purity.

From Fig. 5, it is evident that the VPSA with a vacuum pressure of 0.08 bar achieves CO maximum purity as high as 99.0%. In contrast, the vacuum pressure of about 0.20 bar gives a CO purity of approximately 94.0 % which may be suitable for specific applications. Fig. 5(b) shows the corresponding maximum and average purities in the 0.07-0.2 bar vacuum pressure ranges for a fixed number of cycles of the VPSA. On average, the purity drops as the vacuum pressure increases from 0.07 bar up to 0.2 bar. Here one can deduce that the vacuum pressure of 0.08 bar gives an acceptable CO purity of about 98 %. The effect of change in feed temperature on the CO purity for the configured VPSA seems to be minimal and the CO purity essentially remains constant.

3.3 CO_2 separation from BFG

The CO_2 adsorption bed configuration and isotherm parameters was based on previous works by Brea *et al.* [26], and Park *et al.* [27],where a single layer bed using Zeolite 13 X was used to produce high-purity CO_2. The VPSA was configured to operate under vacuum pressure conditions. The bed data was assimilated from the cited literature [26,27]. In the current work, a product purity of 98% and 90% recovery was obtained at 0.9 bar vacuum pressure. The isotherm type used, along with the parameters applied, are summarised in Table 7.

Table 7: Isotherm configuration for CO_2 VPSA.

Isotherm Type	**Zeolite 13X, Langmuir - 3**			
Component	**IP1**	**IP2**	**IP3**	**IP4**
CH_4	6.39E-03	1.35E-05	3.37E-04	1768.5
CO	0.008035	2.07E-05	4.12E-02	758.5
CO_2	1.15E-02	2.38E-05	1.78E+00	203
H_2	4.69E-03	9.61E-06	2.41E-03	425.2
N_2	4.81E-03	6.68E-06	5.71E-04	1531

The type of isotherm used in the simulation was Langmuir – 3 (equation 6 above). Breakthrough curves were obtained from the experimental work of Brea *et al.* [26] where the simulated time-dependent reactor outlet composition were validated against experimental results and show good agreement as shown in Fig. 6(a).

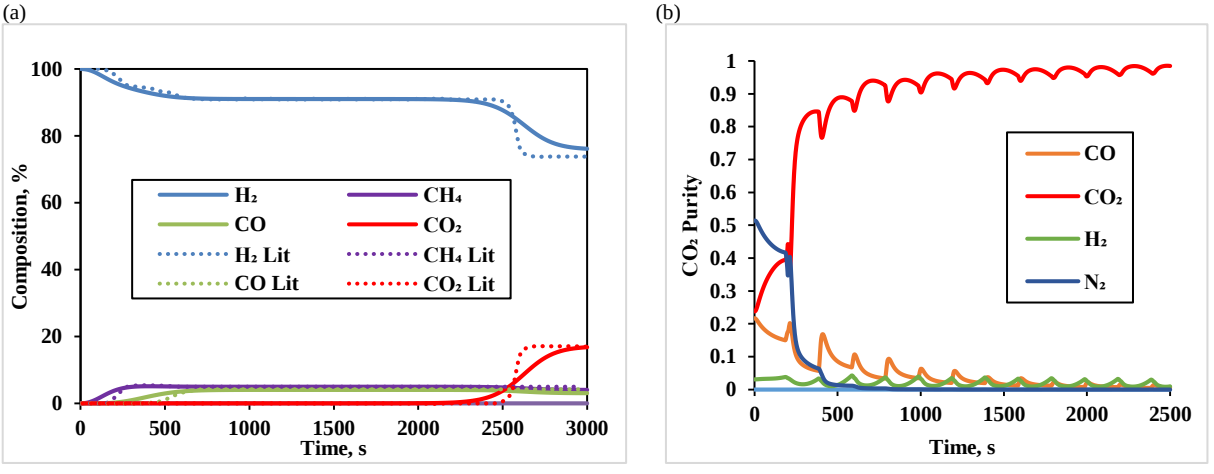

Fig. 6. (a) Breakthrough validation of gases on Zeolite 13X and (b) concentration profile of a CO_2 VPSA over time.

As this simulation is run under a dynamic state, it takes some time before achieving a steady state from initial conditions. It can be seen in Fig. 6(b) that there is a considerable difference in the behaviour in the first two cycles of the PSA, this is because the initial conditions where the bed is not saturated with the feed and is yet to change to steady-state conditions when the simulation starts running.

3.3.1 Parametric analysis

In this case, the set-up was configured for vacuum pressure conditions at below the atmospheric pressure and varied between 0.05-0.9 bar. Fig. 7 summarises the results.

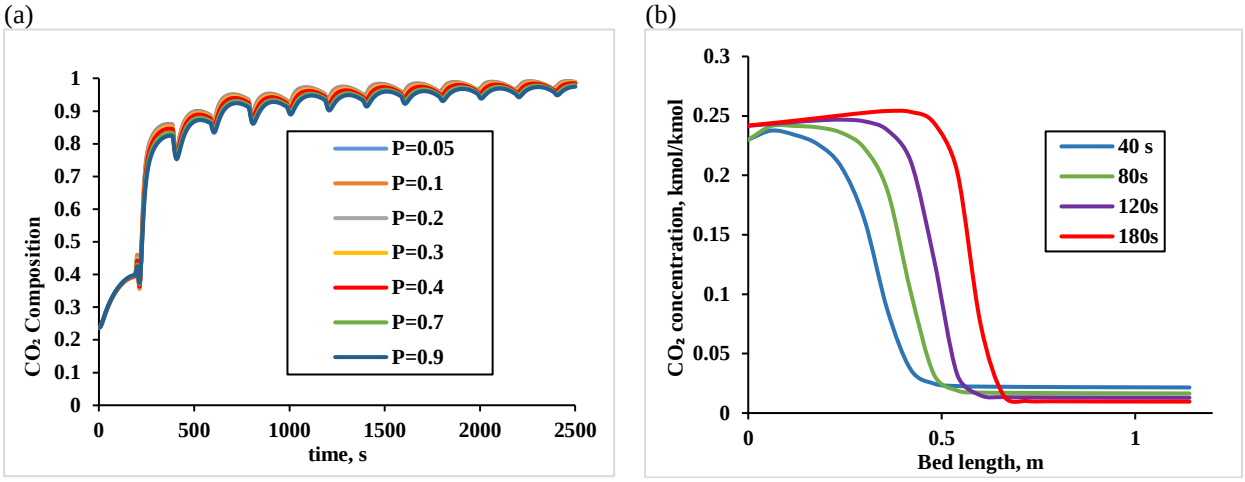

Fig. 7. (a) Effect of vacuum pressure on CO_2 purity and (b) single bed concentration profile of CO_2 as a function of bed length at different adsorption times.

As seen in Fig. 7, the lower the vacuum pressure, the higher the purity of the CO_2. This could be attributed to that fact that more the lower the desorption pressure the more CO_2 desorbs. The difference in purity due to the change in vacuum pressure is however minimal. Hence, to obtain a high CO_2 purity stream, only a low vacuum pressure (of about 0.4 bar) is required. For example, at 0.4 bar vacuum pressure, an average CO_2 purity of 98% is achieved, without unnecessary vacuum pumping costs for 0.1vacuum pressure. With each increase in adsorption step duration from 40 to 180 seconds, the CO_2 concentration front travels up the column, increasing CO_2 content in the effluent (at L = 1.2 m). Also, as the adsorption period increases, more CO_2 is adsorbed; other present components in the incoming feed are displaced by the CO_2, resulting in a bed richer in adsorbed CO_2, which explains the improvement in purity.

The effect of change in feed temperature on the CO_2 purity for the configured VPSA seems minimal, and as with previous cases, the maximum and average CO_2 purity remains relatively unchanged, 25 °C seems to be appropriate, yielding an acceptably high purity CO_2 stream, without added costs associated with increasing the feed temperature.

4. Conclusion

In this work, we present PSA models for the pre-combustion separation of useful components from steelworks off-gases. The separation of these gases using a variation of the Skartsrom cycle, which has been described and discussed. In addition, a parametric analysis was carried out to examine the effect of adsorption and vacuum pressure, temperature and adsorption time on the overall performance of the units. The primary objective was to recover H_2, CO, and CO_2 streams to an acceptable degree of purity. The H_2 PSA unit was a conventional high-pressure PSA operating at 8.5 bar, the CO and CO_2 units were VPSAs, operating at 0.07 bar and 0.4 bar vacuum pressure, respectively. Each of the respective units had different bed configurations, adsorbents, cycle times, pressure conditions (feed and bed pressure or the vacuum pressure) for adsorption/desorption steps.

The findings suggest that the PSA units utilised in this study could be employed to selectively separate high purity streams of H_2 (99.3%), CO (98%) and CO_2 (98%) all with over 90% recovery from steelworks off-gases for both utilisation and sequestration, as required by new clean technologies to produce fuels, chemicals and energy.

Acknowledgement

Support for this research from the Nigerian Petroleum Technology Development Fund (PTDF) is gratefully acknowledged.

References

[1] IEA. Transforming Industry through CCUS. Transform Ind through CCUS 2019. https://doi.org/10.1787/09689323-en.
[2] Holappa L. A General Vision for Reduction of Energy Steel Industry 2020.
[3] Collis J, Strunge T, Steubing B, Zimmermann A, Martin M. Deriving Economic Potential and GHG Emissions of Steel Mill Gas for Chemical Industry 2021;9:1–22. https://doi.org/10.3389/fenrg.2021.642162.
[4] Zhang H, Wang G, Wang J, Xue Q. Recent Development of Energy-saving Technologies in Ironmaking Industry Recent Development of Energy-saving Technologies in Ironmaking Industry 2019. https://doi.org/10.1088/1755-1315/233/5/052016.
[5] Bampaou M, Panopoulos K, Seferlis P, Voutetakis S, Matino I, Iannino V. Integration of Renewable Hydrogen Production in Steelworks Off-Gases for the Synthesis of Methanol and Methane 2021.
[6] Uribe-Soto W, Portha JF, Commenge JM, Falk L. A review of thermochemical processes and technologies to use steelworks off-gases. Renew Sustain Energy Rev 2017;74:809–23. https://doi.org/10.1016/j.rser.2017.03.008.
[7] Lundgren J, Ekbom T, Hulteberg C, Larsson M, Grip CE, Nilsson L, et al. Methanol production from steel-work off-gases and biomass based synthesis gas. Appl Energy 2013;112:431–9. https://doi.org/10.1016/j.apenergy.2013.03.010.
[8] Deng L, Adams TA. Methanol Production from Coke Oven Gas and Blast Furnace Gas. vol. 44. Elsevier Masson SAS; 2018. https://doi.org/10.1016/B978-0-444-64241-7.50022-7.
[9] Danaci D, Webley PA, Petit C. Guidelines for Techno-Economic Analysis of Adsorption Processes 2021;2:1–11. https://doi.org/10.3389/fceng.2020.602430.
[10] Foo KY, Hameed BH. Insights into the modeling of adsorption isotherm systems. Chem Eng J 2010;156:2–10. https://doi.org/10.1016/j.cej.2009.09.013.
[11] Yang J, Han S, Cho C, Lee CH, Lee H. Bulk separation of hydrogen mixtures by a one-column PSA process. Sep Technol 1995;5:23949. https://doi.org/10.1016/0956-9618(95)00128-X.
[12] Casas N, Schell J, Pini R, Mazzotti M. Fixed bed adsorption of CO_2/H_2 mixtures on activated carbon: Experiments and modeling. Adsorption 2012;18:143–61. https://doi.org/10.1007/s10450-012-9389-z.
[13] García S, Gil M V., Pis JJ, Rubiera F, Pevida C. Cyclic operation of a fixed-bed pressure and temperature swing process for CO_2 capture: Experimental and statistical analysis. Int J Greenh Gas Control 2013;12:35–43. https://doi.org/10.1016/j.ijggc.2012.10.018.
[14] Douglas Ruthven, Shamsuzzaman Farooq KK. Pressure swing adsorption. 1993. https://doi.org/10.1016/S0166-9834(00)81410-4.
[15] Baksh et al. Six Bed Pressure Swing Adsorption Process Operating in Normal and Turndown Modes, Us 8,491,704 B2, 2013.
[16] Papadias DD, Ahmed S, Kumar R, Joseck F. Hydrogen quality for fuel cell vehicles - A modeling study of the sensitivity of impurity content in hydrogen to the process variables in the SMR-PSA pathway. Int J Hydrogen Energy 2009;34:6021–35. https://doi.org/10.1016/j.ijhydene.2009.06.026.
[17] Ahn S, You YW, Lee DG, Kim KH, Oh M, Lee CH. Layered two- and four-bed PSA processes for H_2 recovery from coal gas. Chem Eng Sci 2012;68:413–23. https://doi.org/10.1016/j.ces.2011.09.053.
[18] Gao F, Wang S, Wang W, Duan J. Adsorption separation of CO from syngas with CuCl @ AC adsorbent by a VPSA process 2018:39362–70. https://doi.org/10.1039/c8ra08578a.
[19] Abdeljaoued A, Relvas F, Mendes A, Chahbani MH. Simulation and experimental results of a PSA process for production of hydrogen used in fuel cells. J Environ Chem Eng 2018;6:338–55. https://doi.org/10.1016/j.jece.2017.12.010.
[20] Riboldi L, Bolland O. Overview on Pressure Swing Adsorption (PSA) as CO_2 Capture Technology: State-of-the-Art, Limits and Potentials. Energy Procedia 2017;114:2390–400. https://doi.org/10.1016/j.egypro.2017.03.1385.
[21] Khajuria H. Model-based Design, Operation and Control of Pressure Swing Adsorption Systems 2011:1–203.
[22] Fiandaca G, Fraga ES, Brandani S. A multi-objective genetic algorithm for the design of pressure swing adsorption. Eng Optim 2009;41:833–54. https://doi.org/10.1080/03052150903074189.
[23] Ayawei N, Ebelegi AN, Wankasi D. Modelling and Interpretation of Adsorption Isotherms. J Chem 2017;2017. https://doi.org/10.1155/2017/3039817.
[24] Wakao N, Funazkri T. Effect of fluid dispersion coefficients on particle-to-fluid mass transfer coefficients in packed beds. Correlation of sherwood numbers. Chem Eng Sci 1978;33:1375–84. https://doi.org/10.1016/0009-2509(78)85120-3.
[25] Yang J, Lee CH. Adsorption dynamics of a layered bed PSA for H2 recovery from coke oven gas. AIChE J 1998;44:1325–34. https://doi.org/10.1002/aic.690440610.
[26] Brea P, Delgado JA, Águeda VI, Gutiérrez P, Uguina MA. Multicomponent adsorption of H_2, CH_4, CO and CO_2 in zeolites NaX, CaX and MgX. Evaluation of performance in PSA cycles for hydrogen purification. Microporous Mesoporous Mater 2019;286:187–98. https://doi.org/10.1016/j.micromeso.2019.05.021.
[27] Co M, Park Y, Ju Y, Park D, Lee C. Adsorption equilibria and kinetics of six pure gases on pelletized zeolite. Chem Eng J 2016;292:348–65. https://doi.org/10.1016/j.cej.2016.02.046.